PERFORMANCE OF AUTOMATIC TIE POINT EXTRACTION USING HRSC IMAGERY OF THE MARS EXPRESS MISSION

C. Heipke[a], R. Schmidt[a], R. Brand[a], J. Oberst[b], G. Neukum[c] and the HRSC Co-Investigator Team

[a]Institute of Photogrammetry and GeoInformation, University of Hannover, Nienburger Str. 1, D-30167 Hannover, Germany, schmidt@ipi.uni-hannover.de
[b]Institut für Planetenforschung, DLR Berlin, Rutherfordstr. 2, D-12489 Berlin, Germany, juergen.oberst@dlr.de
[c]Institut für Geologie, Geophysik und Geoinformatik, Freie Universität Berlin, Malteserstr. 74-100, D-12249 Berlin, Germany, gneukum@zedat.fu-berlin.de

Commission IV, WG IV/9

KEY WORDS: Extraterrestrial, Planetary, Camera, Matching, Scanner, Multiline, High resolution, Three-Line

ABSTRACT:

In January 2004 the first European interplanetary spacecraft, Mars Express, was inserted successfully into a Martian orbit. The multiline scanner HRSC (High Resolution Stereo Camera) on board of Mars Express will image most of the surface of Mars in colour and stereoscopically in high resolution. The Institute of Photogrammetry and GeoInformation (IPI), University of Hannover, has created software for the automatic extraction of homologous image primitives from HRSC image data. With the obtained tie points a bundle block adjustment will be carried out with software developed at the Chair for Photogrammetry and Remote Sensing (LPF) of the Technische Universität München which will result in an improved exterior orientation of the camera. With these results high level products such as digital terrain models (DTMs), ortho photos and shaded reliefs can be derived from the imagery.
This paper describes the used approach for the tie point matching. On the basis of some selected Mars Express orbits the results of the matching, the distribution of the tie points in the images and the achieved accuracy are presented and evaluated.

1. INTRODUCTION

In June 2003 the European Space Agency (ESA) launched the Mars Express spacecraft from the Baikonur launch pad in Kazakhstan. After a journey of about six months the orbiter was successfully inserted into a polar orbit around Mars. During its two years mission the HRSC on board of Mars Express images large parts of the Mars surface. The HRSC is a multisensor pushbroom camera consisting of nine charge coupled device (CCD) line sensors mounted in parallel for simultaneous high resolution stereo, multispectral, and multiphase imaging (Albertz et al., 1993). At pericenter about 300 km above the surface of Mars a ground resolution of about 12 m is attained. The Camera Unit (CU) of the HRSC additionally comprises a Super Resolution Channel (SRC) which captures frame images embedded in the basic HRSC swath at a ground resolution of up to 2.5 m.

The three-dimensional position and attitude of the spacecraft is constantly determined by ESA by combining techniques of measuring Doppler shifts, acquiring ranging data, triangulation measurements and a star tracker camera. These measurements result in a three-dimensional position and attitude of the spacecraft over time which can be considered as approximate exterior orientation in classical photogrammetry. However, these values are not consistent enough for high accuracy photogrammetric point determination. Therefore, a bundle adjustment has to be performed using these values as direct observations for the unknown exterior orientation parameters. In addition to these observations automatically extracted tie points derived via digital image matching (DIM) are used as input for the bundle adjustment. For every orbit, where HRSC imagery exists, IPI and LPF are jointly processing the HRSC data. The tie points are obtained by software developed at IPI (Schmidt, Brand, 2003) and the image coordinates of the tie points are sent to LPF as input for the bundle adjustment (Ebner et al., 2004). The mapping performance of the HRSC is analysed in (Oberst et al., 2004).

The interior orientation of the HRSC has been calibrated in a laboratory at Dornier, Friedrichshafen and has been verified during the six months journey to Mars by means of star observations. So far no deviations from the calibration have been experienced so that the interior orientation of the HRSC is considered to be stable.

In section two of this paper the approach used for the generation of tie points from HRSC imagery is presented. In section three the test data is described and the results of the tie point matching derived from some selected orbits are shown and discussed. The last section summarises the results and some conclusions are drawn.

2. MATCHING APPROACH

Our matching approach follows a coarse to fine strategy which means the matching result is refined step by step through image pyramids. As input data the HRSC imagery, the observed exterior orientation and the calibration data of the interior orientation are needed. As an optional input it is possible to use a DTM as approximate information. On Mars a high accuracy DTM derived from data of the MOLA instrument (Neumann et al., 2003) is available.

At first point features are extracted using the Förstner operator (Förstner, 1986) and the images are matched pairwise in all combinations using the cross correlation coefficient as

similarity measure. Each image is divided into subareas to ensure an even distribution of the tie points over the whole area. To reduce ambiguities and computing time the matching location and a search space for the corresponding feature has to be determined. The principle of the transformation from object to linescanner coordinates is described in Dörstel, Ohlhof (1996). Since no epipolar geometry exists for linescanner imagery a feature in one image is transferred to the next image via the collinearity equations for 3-line imagery (1) according to the extended functional model of Ebner et al. (1994).

$$\begin{pmatrix} x - x_0 \\ y - y_0 \\ -c \end{pmatrix} = \lambda M^T(\Delta\varphi, \Delta\omega, \Delta\kappa) D^T(\varphi, \omega, \kappa) \left[\begin{pmatrix} X \\ Y \\ Z \end{pmatrix} - \begin{pmatrix} X_0 + \Delta X_0 \\ Y_0 + \Delta Y_0 \\ Z_0 + \Delta Z_0 \end{pmatrix} \right] \quad (1)$$

with

$$\begin{pmatrix} \Delta X_0 \\ \Delta Y_0 \\ \Delta Z_0 \end{pmatrix} = D(\varphi, \omega, \kappa) \begin{pmatrix} \Delta x \\ \Delta y \\ \Delta z \end{pmatrix} \quad (2)$$

The exterior orientation refers to a camera coordinate system common to all CCD lines and is expressed for a given readout cycle n as X_0, Y_0, Z_0, φ, ω, κ (Figure 1). The interior orientation parameters x_0, y_0, c are defined in the image coordinate system, three separate values exist for each line. The transformation between the image coordinate system and the camera coordinate system is given by Δx, Δy, Δz, Δφ, Δω, Δκ, which have been determined in the geometric calibration for each line separately. M as well as D are rotation matrices, λ is a scale factor. The image coordinates are given by x and y, which are derived automatically in this case via DIM.

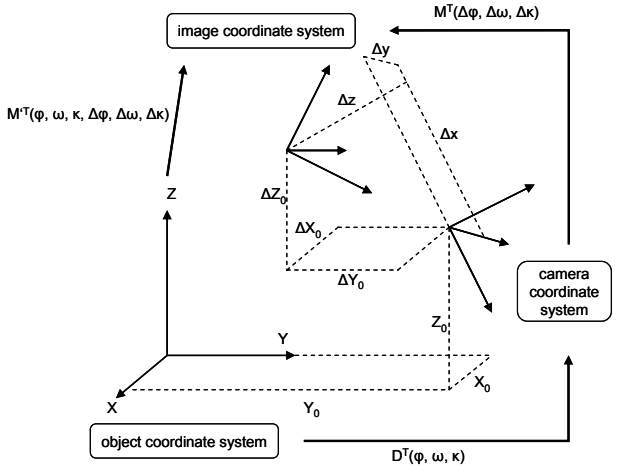

Figure 1: Coordinate systems (according to Kornus, 1999).

For the transformation from object space to image space as a function of the image line (readout cycle) *n* the additional condition (3) has to be applied.

$$x(n) = x\left(n, X_0(n), Y_0(n), Z_0(n), \varphi(n), \omega(n), \kappa(n)\right) = 0 \quad (3)$$

This problem can be solved using the well known Newton-method for the above zero-crossing detection where the derivative $x'(n_i)$ is replaced by the pixelsize of the image.

$$\begin{aligned} n_0 &= \textit{initial value for the image line} \\ n_{i+1} &= n_i - x(n_i) / \textit{pixelsize} \quad i = 0,1,\ldots \end{aligned} \quad (4)$$

The principle of transforming a feature from one image to the next is shown in Figure 2. The point P (extracted feature P') has an estimated elevation Z_P taken from the MOLA DTM, where Δz denotes the uncertainty of this value. This defines a range U, L that is projected to the right image where it defines the search space s.

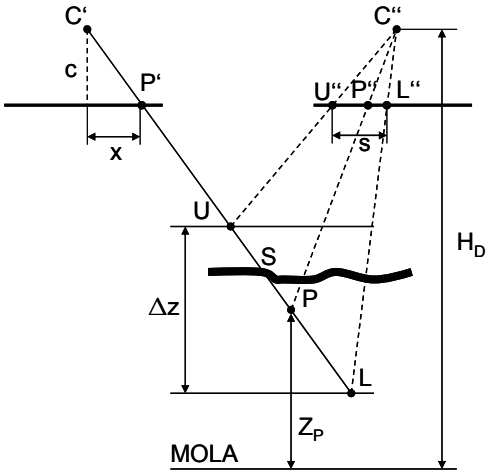

Figure 2: Principle of estimating matching location and search space (according to Schenk, 1999).

After matching all overlapping images pairwise in all combinations an undirected graph is generated. The nodes of the graph are the point features, the edges are the matches between them. This graph is divided into connected components. The next step is the generation of point tuples, whereas one point tuple is characterised by the property that not more than one feature per image is admissible. The complexity of this problem can grow exponentially. Instead of using tree search or binary programming techniques a RANSAC (Random Sample Consensus) procedure (Fischler, Bolles, 1981) is applied. The method relies on the fact that the likelihood of hitting a good configuration (correct tuple) by randomly choosing a set of observations (features of the subgraph) is large after a certain number of trials. The advantage of this method is the high probability of getting a good point. Including a geometric consistency check, the method also eliminates blunders (Brand, Heipke, 1998).

From the start pyramid level (lowest resolution) to the so-called intermediate level (medium resolution) feature based matching (FBM) is carried out using the whole images. For the processing of the HRSC imagery level 3 has been chosen as starting level. Going down the image pyramid the image size increases, as well as the number of extracted features. Besides the heavily increasing computational time, the matching of the complete images would result in too many tie points for the camera orientation. Therefore the matching procedure is carried out only for selected "image chips", starting at pyramid level 2.

This means that corresponding points are searched in areas only where points have been found before due to good texture (Tang, Heipke, 1996).

To further refine the result Multi Image Least Squares Matching (MILSM) is carried out following the approach of Krupnik (1994). In this method the tie points are matched in all images simultaneously. Because it is the most accurate matching technique available it is possible to further refine the result of the feature based matching. In our implementation we can decide whether to apply MILSM or not for each pyramid level. To save computing time it is advisable to carry out MILSM only on the last level, which represents the original resolution. In this approach the affine transformation parameters between areas defined around the matching location called image patches are determined in an arbitrary number of images. In order to avoid a datum defect, one image patch has to be fixed serving as reference for the other patches. The least squares adjustment can be described by

$$\begin{aligned} v &= \hat{G} - g(\hat{p}) \\ &= G_0 + d\hat{G} - \left(g(p_0) + \frac{\partial g}{\partial p} d\hat{p} \right) \\ &= -\frac{\partial g}{\partial p} d\hat{p} + d\hat{G} - \left(g(p_0) - G_0 \right) \end{aligned} \tag{5}$$

where v denotes the residuals, G the theoretical grey values computed as mean value from all image patches at (r, c), $g(p)$ the grey values of the image patches, p the affine transformation parameters between the image patches, $d\hat{G}$ the unknown differences to the initial value for the theoretical grey values, $d\hat{p}$ the unknown corrections for the parameters and the subscript 0 stands for initial values of the unknowns. One such equation can be set up for every pixel of the reference patch transformed into every available image. The discretisation of equation (5) leads to the following linear system:

$$\begin{aligned} v = &-g_r^i(r,c)\,d\hat{a}_1^i - g_c^i(r,c)\,d\hat{a}_2^i \\ &-g_r^i(r,c)\,d\hat{a}_3^i - g_r^i(r,c)\,d\hat{a}_4^i \\ &-g_c^i(r,c)\,d\hat{a}_5^i - g_c^i(r,c)\,d\hat{a}_6^i \\ &+d\hat{G}(r,c) - g^i(r,c) + G_0(r,c) \\ v = &\; d\hat{G}(r,c) - g^0(r,c) + G_0(r,c) \end{aligned} \tag{6}$$

where i denotes the number of the image patch, r the row– and c the column coordinates of the image patch. The used symbols are described in the following:

$g^i(r,c)$	grey value of image patch *i (i = 1, …, n)* at *r, c*
$g^0(r,c)$	grey value of fixed reference image patch 0 at *r, c*
g_r^i	grey value gradient of image patch *i* w.r.t. *r*
g_c^i	grey value gradient of image patch *i* w.r.t. *c*
$G_0(r,c)$	initial value of theoretical grey value at *r,c*
da_1^i, da_2^i	unknown shift parameters between image patch *i* and reference image patch 0
$da_3^i, ..., da_6^i$	unknown rotation and shear parameters between image patch *i* and reference image patch 0
$dG(r,c)$	unknown change of theoretical grey value at r, c

It is also possible to choose whether to use all six unknown parameters $da_1^i, ..., da_6^i$ for the MILSM or only the two shift parameters da_1^i, da_2^i.

Finally, model points are derived via forward intersection of the image coordinates of the tie points. They serve as an approximation for the reduction of the search space on the next lower pyramid level instead of the MOLA points. The MOLA DTM is used only on the first pyramid level. The application flow of the matching is shown in Figure 3.

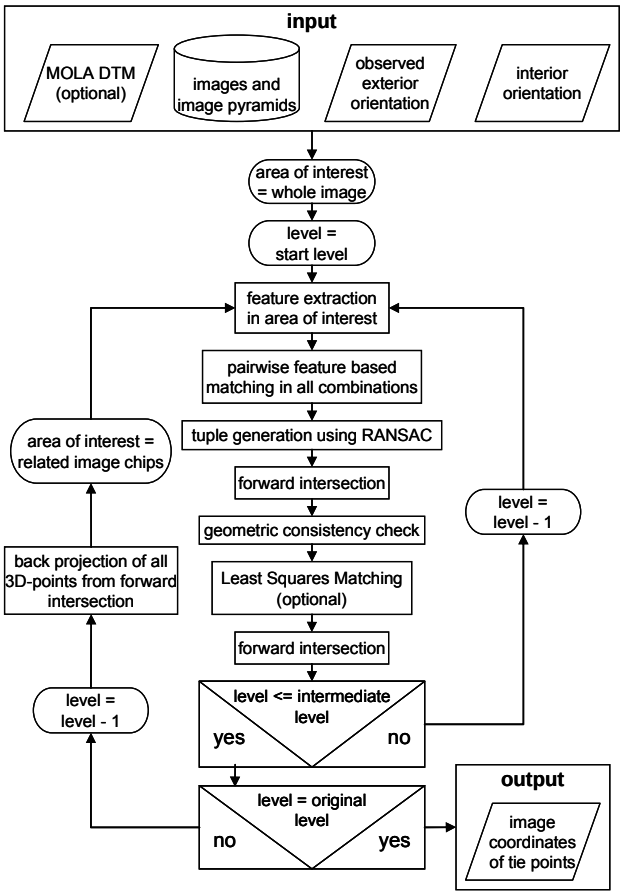

Figure 3: Application flow of the matching.

3. RESULTS

In this section, first the used HRSC imagery will be described. In the second part the results of the matching will be presented and discussed on the basis of the orbits 18, 22 and 68.

3.1 Data

For the evaluation of the matched tie points, imagery of the orbits 18, 22 and 68 have been chosen which have been received in the early phase of the Mars Express mission. Besides the HRSC imagery, the observations of the exterior

orientation and the calibration data of the interior orientation as well as the MOLA DTM are used as input for the DIM.

The CCD arrays of the HRSC consist of 5176 active pixels each, which yields a swath width of about 65 km on the surface of Mars. The strips can have a length of up to 300.000 lines, spanning about 4.000 km on the surface. Due to a limited bandwidth between Mars and Earth only the nadir channel is able to operate at full resolution. Generally the resolution of the two stereo channels has to be reduced by a factor of 2 and the remaining channels by a factor of 4. To obtain an equivalent scale the nadir channel has to be resampled to the resolution of the stereo channels for the matching. Depending on the covered region on Mars the imagery shows areas with high texture and areas with hardly any texture (Figure 4).

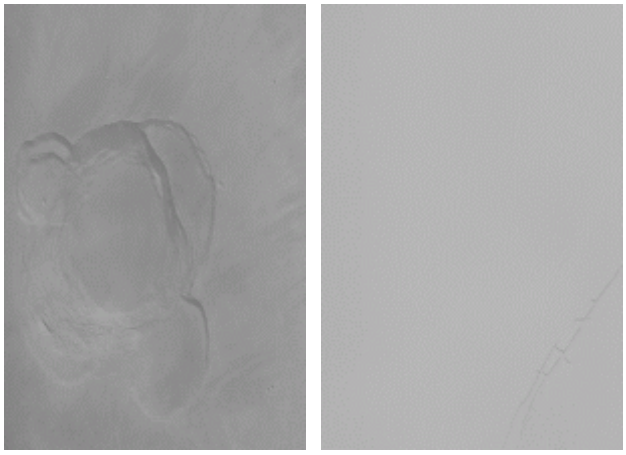

Figure 4: Left: Part of orbit 68 with good texture. Right: Part of orbit 68 with very low texture.

The matching was carried out on the original level-2 data (Roatsch, 2000) which means no geometric corrections have been applied to the imagery prior to matching. Since the minimal flying altitude of the spacecraft is about 300 km above the surface the spacecraft isn't exposed to turbulences which aerial cameras here on earth experience. Thus the spacecraft moves with hardly any disturbances along its trajectory resulting in imagery without jitter.

In orbit 22 the two photometry channels were also available at the same resolution as the stereo channels and were used for the matching resulting together with the nadir channel in five overlapping strips.

3.2 Results

In a first evaluation the distribution of the tie points in the image strip is evaluated. In Figure 5 it is noticeable that the tie points are evenly distributed over the whole image strip. Most of them are 3-fold points. There are some areas visible which don't contain any point. This doesn't pose a problem for the determination of the absolute orientation because the used approach (Ebner et al., 2004) shifts the trajectory on the whole by applying six biases, one for every element of the exterior orientation. Even in orbit 68, with large empty areas due to low texture (Figure 4), we were able to determine the exterior orientation of the camera. Problems raise at determining a DTM in those areas using image matching methods.

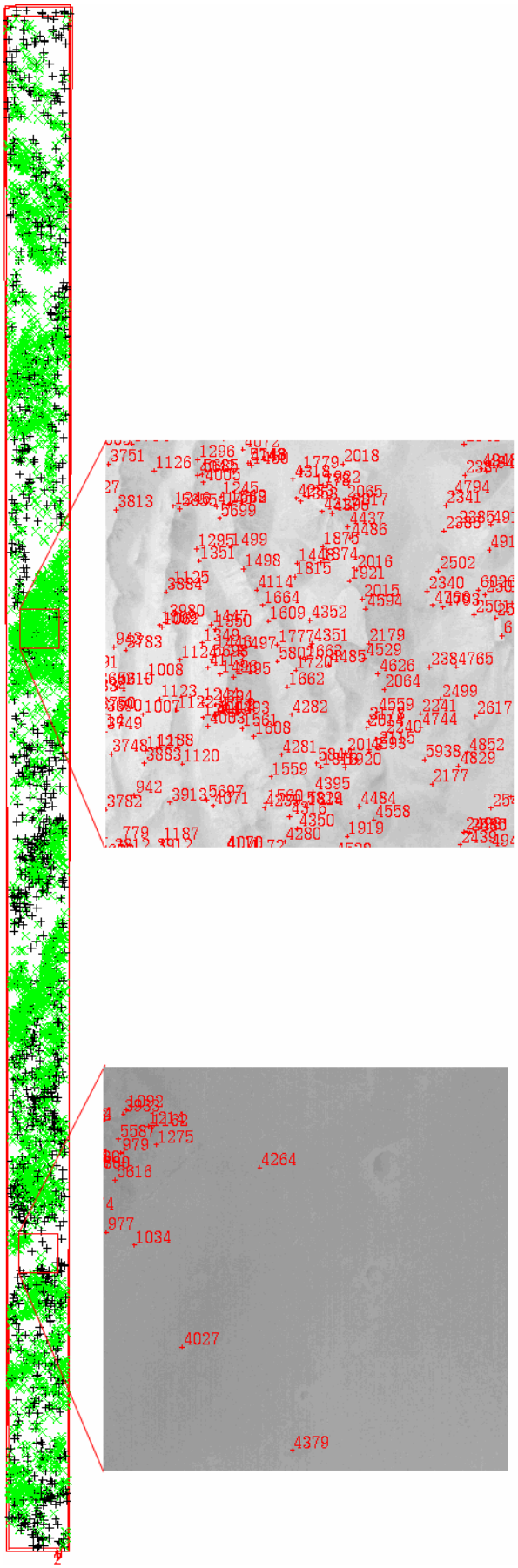

Figure 5: Distribution of the tie points in orbit 18. + 2-fold, x 3-fold point, north is up

After the visual evaluation of the tie points the accuracy of the ray intersections was analysed. First, the values of the exterior orientation from ESA have been fixed in the bundle adjustment and no DTM as control information has been introduced. This can be considered as a forward intersection. In Table 1 the theoretical standard deviations of the object coordinates of the ray intersections are shown for the selected orbits. Only 3-fold points have been used for all computations.

orbit	altitude [km]	σX [m]	σY [m]	σZ [m]
18	275 – 347	12.9	11.0	34.3
22	311 – 941	13.2	18.1	42.2
68	269 – 505	30.3	27.6	48.7

Table 1: Theoretical standard deviations of the object coordinates of the ray intersections using ESA exterior orientation.

Table 2 shows the results after automatically removing some matching blunders. Compared to the values given in Table 1 the differences of the standard deviations are not significant.

orbit	altitude [km]	σX [m]	σY [m]	σZ [m]
18	275 – 347	12.1	10.7	33.4
22	311 – 941	13.0	17.2	41.6
68	269 – 505	31.2	29.2	50.6

Table 2: Theoretical standard deviations of the object coordinates of the ray intersections after removing some matching blunders.

The obtained values are compared to the results calculated by a bundle adjustment improving φ and κ (Table 3). This means a constant bias is estimated for both angles along the entire orbit. Biases for φ and κ were introduced, because only these two parameters can be improved using tie points. Biases for the other four orientation parameters X0, Y0, Z0 and ω can only be determined based on ground control information. Here some points have also been eliminated as blunders. As can be seen the bundle adjustment yields higher quality tie points and higher achievable accuracy of the ray intersections.

orbit	altitude [km]	σX [m]	σY [m]	σZ [m]
18	275 – 347	6.6	6.0	18.1
22	311 – 941	8.6	9.1	21.9
68	269 – 505	11.0	10.4	17.9

Table 3: Theoretical standard deviations of the object coordinates of the ray intersections after improving φ and κ.

The standard deviations of the object points are in a range of about 6 to 11 m in X and Y, depending on different imaging altitudes. Z accuracies of all orbits are about 18 to 22 m. The standard deviations of the ray intersections are improved by a factor of 2 to 3. Presuming a pixel size of about 25 m on the surface, a final accuracy of about 0.4 pixel in X and Y and 0.8 pixel in Z is achieved.

In Table 4 the changes of the standard deviation on each pyramid level of orbit 18 are shown. Here the standard deviations have been calculated using the fixed exterior orientation like in Table 1. As expected the accuracy of the tie points increases from level to level. Table 5 shows the standard deviations after the bundle adjustment. It can be seen that on each level the standard deviation can be improved by a factor of about 2 and the best results are achieved on the original level.

level	number of points	fixed exterior orientation [m]		
		σX	σY	σZ
L3	5474	98.4	83.9	258.9
L2	11658	35.6	30.2	93.1
L1	10548	22.0	18.6	57.2
L0	4757	14.3	12.1	37.4

Table 4: Progression of the standard deviation on each pyramid level of orbit 18 using a fixed exterior orientation.

level	number of points	improved φ and κ [m]		
		σX	σY	σZ
L3	4216	43.6	38.5	116.2
L2	8488	25.4	22.2	67.8
L1	6457	14.5	12.8	39.1
L0	3776	6.6	5.9	18.0

Table 5: Progression of the standard deviation on each pyramid level of orbit 18 after improving φ and κ.

Finally, the number of 5-fold points and the standard deviations after adjusting φ and κ using different LSM modes are presented in Table 6 considering orbit 22 as example. In the first line the result without LSM is shown. More than 5.000 5-fold points have been derived via FBM. In LSM mode A all six affine parameters of the least squares adjustment have been used.

LSM mode	number of 5-fold points	σX [m]	σY [m]	σZ [m]
no	5533	11.3	11.8	26.4
A	96	7.9	13.3	19.6
B	1648	9.1	7.6	21.6
C	1648	9.1	7.6	21.6

Table 6: Number of 5-fold points and accuracies using different LSM modes in orbit 22.

It can be seen that the standard deviations of the ray intersections have been improved by applying LSM. However, the number of 5-fold points decreased to 96. By accounting only for the two shift parameters in the adjustment (LSM mode B) 1648 5-fold points have been obtained and the standard deviations lie in a similar range as for mode A. This seems to be a sufficient number for the bundle block adjustment.

It is also possible to use a combination of the LSM modes A and B (LSM mode C), where the result of the two shift parameters are used as approximate values for the adjustment applying all six parameters. Admittedly this method yields no advantage in the investigated case. However, it has to be stated that this is no recommendation for using only the two shift parameters in every case. Further investigations will be carried out evaluating these LSM modes with different imagery.

4. CONCLUSIONS

The results show the efficiency of the image matching approach for the generation of tie points. The tie points are distributed evenly over the whole block with a good rate of manifold points. An accuracy of 0.4 pixel in position and 0.8 in height is achieved. Using a bundle adjustment the ray intersections could be improved by a factor of 2 to 3.

Also the LSM is able to further improve the results by refining the FBM and eliminating suboptimal points. In this case of planetary imagery it has been found so far that it is reasonable to use only two shift parameters for the LSM instead of all six affine parameters.

In areas with very low texture only few points have been found which doesn't pose a problem for the determination of the exterior orientation of the camera. Problems raise when a DTM needs to be generated in those areas using image matching methods. Applying shape from shading can help to close gaps in the DTM in areas with low texture (Lohse, Heipke, 2003), and we will investigate the combination of both methods in the future.

5. REFERENCES

Albertz, J., Scholten, F., Ebner, H., Heipke, C., Neukum, G., 1993. Two camera experiments on the Mars 94/96 missions, *Geo-Informations-Systeme*, (6) 4, pp. 11-16.

Brand, R., Heipke, C., 1998. A system for automatic aerial triangulation, *IntArchPhRS*, (32) 2, pp. 27-32.

Dörstel, C., Ohlhof, T., 1996. Processing and display of three-line imagery at a digital photogrammetric workstation, *IntArchPhRS*, (31) 2, pp. 72-77.

Ebner, H., Kornus, W., Ohlhof, T., 1994. A simulation study on point determination for the MOMS-02/D2 space project using an extended functional model, *Geo-Informations-Systeme*, (7) 1, pp. 11-16.

Ebner, H., Spiegel, M., Baumgartner, A., Giese, B., Neukum, G., and the HRSC Co-Investigator Team, 2004. Improving the exterior orientation of Mars Express HRSC imagery, *IntArchPhRS*, (35).

Fischler, M. A., Bolles, R. C., 1981. Random Sample Consensus: A paradigm for model fitting with applications to image analysis and automated cartography, *Communications of the ACM*, (24), 6, pp. 381-395.

Förstner, W., 1986. A feature based correspondence algorithm for image matching, *IntArchPhRS*, (26) 3/3, pp. 150-166.

Kornus, W., 1999. Dreidimensionale Objektrekonstruktion mit digitalen Dreizeilenscannerdaten des Weltraumprojekts MOMS-02/D2, *DGK-C*, (496), München.

Krupnik, A., 1994. Multiple-patch matching in the object space for aerotriangulation, *Technical Report 428,* Department of Geodetic Science and Surveying, The Ohio State University, Columbus.

Lohse, V., Heipke, C., 2003. Derivation of digital terrain models by means of multi-image shape-from-shading: Results using Clementine images, *ISPRS Workshop High Resolution Mapping from Space 2003*, October 6-8, 2003, Hannover.

Neumann, G. A., Lemoine, F. G., Smith, D. E., Zuber, M. T., 2003. The Mars Obiter Laser Altimeter archive: Final precision experiment data record release and status of radiometry, *Lunar Planet. Sci. XXXIV*, Lunar and Planetary Institute, Houston.

Oberst, J., Roatsch, T., Giese, B., Wählisch, M., Scholten, F., Gwinner, K., Matz, K.-D., Hauber, E., Jaumann, R., Albertz, J., Gehrke, S., Heipke, C., Schmidt, R., Ebner, H., Spiegel, M., vanGasselt, S., Neukum, G., and the HRSC Co-Investigator Team, 2004. The mapping performance of the HRSC / SRC in Mars orbit, *IntArchPhRS*, (35).

Roatsch, T., 2000. HRSC Level-2 product description, *internal report*, DLR, Berlin.

Schenk, T., 1999. *Digital Photogrammetry Vol. 1*, TerraScience, Laurelville, p. 244.

Schmidt, R., Brand, R., 2003. Automatic determination of tie points for HRSC on Mars Express, *ISPRS Workshop High Resolution Mapping from Space 2003*, October 6-8, 2003, Hannover.

Tang, L., Heipke, C., 1996. Automatic relative orientation of aerial images, *PE&RS*, (62), 1, pp. 47-55.

6. ACKNOWLEDGEMENTS

This work is funded by Deutsches Zentrum für Luft- und Raumfahrt e.V. (DLR) under grant no. 50 QM 0104. This support is gratefully acknowledged.